Loss and Energy Determination of a 400 kW Grid-Connected Supercapacitor Energy Storage System

1st Michael Hetzel
Elektrotechnisches Institut (ETI)
Karlsruhe Institute of Technology (KIT)
Karlsruhe, Germany
michael.hetzel@kit.edu

2st Lukas Stefanski
Elektrotechnisches Institut (ETI)
Karlsruhe Institute of Technology (KIT)
Karlsruhe, Germany
lukas.stefanski@kit.edu

3st Marc Hiller
Elektrotechnisches Institut (ETI)
Karlsruhe Institute of Technology (KIT)
Karlsruhe, Germany
marc.hiller@kit.edu

***Abstract*—This paper presents a 400 kW grid-connected supercapacitor energy storage system. The losses of the active Front End including an LCL filter, the DC/DC converter, the supercapacitor storage and the overall system are measured and possibilities to decrease them are identified. Mathematical descriptions of converter losses are presented and combined with a modeling approach for the supercapacitor storage. The resulting model describes the power flows and losses within the overall system as a function of the terminal behavior of the supercapacitor storage.**

***Index Terms*—supercapacitor, loss estimation, energy storage system**

I. Introduction

Electrical energy storage systems (ESS) are playing an increasingly important role in low-voltage grids [1]–[3]. For the selection of suitable energy storage systems, the characteristics of the storage technology must be known with sufficient accuracy. The influence of inverters, controlling the power flow between energy storage and grid can also not be neglected in this context. The converters influence efficiency and maximum power of the overall system.

In this work, the operational behavior of a 400 kW Supercapacitor Energy Storage System (SCESS) and its grid connection to the 400 V low-voltage grid are investigated. The influences of power losses on the system and possibilities to decrease them are shown. Section 2 presents the overall system consisting of a Supercapacitor Energy Storage (SCES), a DC/DC converter and the Active Front End (AFE) with an LCL filter connecting to the low voltage AC grid. Section 3 presents an approach for modeling the losses of the AFE, DC/DC converter and the SCES. Section 4 describes the measurements performed and the derived power losses of the system components. Based on the modeling approach the system behavior of the SCESS for constant power operation is presented in Section 5.

II. Hardware Platform

In Fig. 2 a schematic overview of the complete test bench consisting of an LCL-filter, an AFE based on a two-level inverter, a three-phase interleaved DC/DC converter and the SCES itself is presented. The AFE regulates the DC link voltage u_{DCB} to a constant voltage of 600 V. The DC/DC converter controls the power flow between the AFE and the SCES. The half-bridges of the DC/DC converter can be switched off depending on the operating point to reduce losses. The phase offset between the half-bridges is selected depending on the number of active half-bridges to minimize the resulting current ripple in the SCES. The SCES is designed with three parallel branches, each consisting of 240 Supercapacitors (SC) connected in series. Each SC has a nominal capacitance of 3000 F and a rated voltage of 2.7 V. They are passively balanced via parallel resistors and actively balanced above a cell voltage of 2.5 V. The theoretical capacitance of the SCES equals 37.5 F with a maximum voltage of 600 V and a theoretically stored energy of 1.88 kWh. The overall system requires 12 s for charging and 14.2 s for discharging between 100 V and 540 V at maximum power of 400 kW. A modular signal processing system based on the ZYNQ7030 System-on-Chip (SoC) from Xilinx [4] is controlling the test bench. A picture of the test bench is shown in Fig. 1. The specification of the test bench is summarized in Tab. I. The test bench is part of the Energy Lab 2.0 [5] in which different forms of energy storage systems are investigated.

Fig. 1: Test bench.

III. Loss Approximation

1) Approximation of the Converter Losses: The dominant losses in hard-switching converters are the switching and conduction losses of the semiconductors. Here, the switching losses have an approximately linear dependence on current

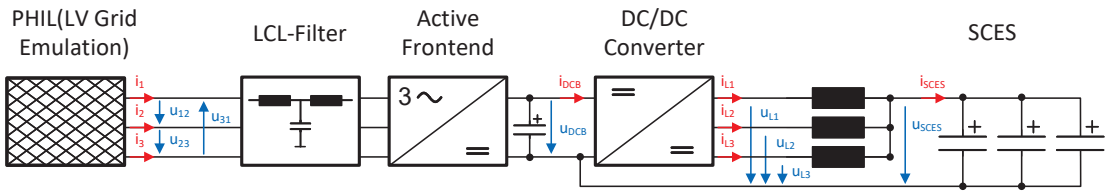

Fig. 2: System overview of the SCESS with converters, grid connection and the SCES.

TABLE I: Characteristics of the test bench

AFE		DC/ DC Converter		SCES	
s_{rated}	630 kVA	p_{rated}	500 kW	p_{rated}	400 kW
$u_{DCB,max}$	720 V	$u_{DCB,max}$	720 V	$u_{SCES,max}$	550 V
$i_{AC,max}$	1358 A	$i_{Ln,max}$	500 A	$i_{SCES,max}$	1400 A
$i_{DCB,max}$	1506 A	$i_{DCB,max}$	1004 A	$e_{SCES,nom}$	~1 kWh

if the voltage is constant [6]. For IGBTs, the conduction losses have a component that is linearly dependent and one that has a quadratic dependence on current [6]. Furthermore, there are additional losses in other components such as diodes and inductors or due to the load current ripple. Therefore, to reduce the model complexity, the converter losses of the AFE with LCL filter and the DC/DC converter are approximated by second degree polynomials, which are defined section-wise for positive and negative input value.

$$y(x) = \begin{cases} ax^2 + bx + c & x > 0 \\ dx^2 + ex + f & x <= 0 \end{cases} \quad (1)$$

Considering the AFE, however, its loss characteristic is not determined in relation to the grid current, but in relation to the DC link power. This is possible because the DC link power is proportional to the grid current if a fixed grid voltage is assumed and the AFE losses are neglected. The DC/DC converter has a three-phase design, with a rated current i_{Lx} of 500 A for each phase. Therefore, one or more half-bridges can be switched off depending on the current, which changes the losses of the DC/DC converter. Hence, there are three different characteristic curves which describe the losses for the DC/DC converter depending on the number of active half-bridges. The second degree polynomials for the loss approximation are shown in Tab. II. Here $p_{l,AFE}$ corresponds to the model losses of the AFE and $p_{l,DCDC,xhb}$ corresponds to the model losses of the DC/DC converter with one to three active half-bridges. The parameters were determined using a least-squares approximation. The data used for the determination is described in Sec. IV-2.

2) Approximation of the Losses of the SCES: Most publications on the loss determination of SCES calculate the power losses assuming that the SCES consists of an ideal capacitance with a series resistor [7]. In [8], the power losses in the frequency domain are also determined and compared with the power losses in the time domain. However, these approaches neglect additional effects, such as charge redistribution, or the increase of the real part of the impedance at very low frequencies. To account for these effects, time-dependent modeling is necessary. In [9], the impedance of the SCES is determined for the test bench presented in this paper and a model of the test bench for determining the voltage of the SCES is parameterized using a nonlinear least squares method and the determined impedance of the SCES. In this paper the model from [9] is extended by a leakage resistance R_{leak} and used to determine the losses in the SCES. Fig. 3 shows the extended model. Its parameters are given in Tab. III. The capacity C_0 is equal to:

$$C_0 = k_0 \cdot u_{C0} + C_{0,const} \quad (2)$$

Here u_{C0} corresponds to the voltage across C_0. $C_{0,const}$ is the capacitance of C_0 at $u_{C0} = 0\,V$. k_0 is a constant of proportionality with which C_0 changes as a function of u_{C0}. To determine the losses of the model, a vector of the measured current values averaged over one pulse period with $T_A = 125\,\mu s$ is applied. Therefore, the losses due to current ripple are not taken into account. The initial voltage of the model capacitors C_0, $C_{p,1}$ and $C_{p,2}$ were chosen according to the starting voltage. The voltage $C_{s,1}$ was set to zero volt. This corresponds to the assumption that the entire model is in steady state. The model losses equal the losses in the model resistors.

3) Resulting Power Loss Model: The previous loss considerations can now be used to determine the losses of the AFE, the DC/DC converter and the SCES. The losses are only in dependence of the voltage and current of the SCES u_{SCES} and i_{SCES}, respectively, to determine the power at the grid, in the DC bus, or the internal power of the SCES.

$$p_{SCES,internal} = u_{SCES} \cdot i_{SCES} - p_{l,SCES}(i_{SCES}) \quad (3)$$

$$p_{DCB} = p_{l,DCDC}(i_{SCES}) + u_{SCES} \cdot i_{SCES} \quad (4)$$

$$p_{grid} = p_{DCB} + p_{l,AFE}(p_{DCB}) \quad (5)$$

Since the model of the SCES can be used to determine not only the losses but also its terminal voltage, all powers and losses

TABLE II: Functions for modeling the power losses of the AFE and the DC/DC converter.

$$
\begin{aligned}
p_{\mathrm{l,AFE}} &= \begin{cases} 18.45\,\frac{1}{\mathrm{GW}} \cdot {p_{\mathrm{DCB}}}^2 + 6.31 \times 10^{-3} \cdot p_{\mathrm{DCB}} + 3.37\,\mathrm{kW}, & p_{\mathrm{DCB}} \geq 0\,\mathrm{W} \\ 14.65\,\frac{1}{\mathrm{GW}} \cdot {p_{\mathrm{DCB}}}^2 - 4.55 \times 10^{-3} \cdot p_{\mathrm{DCB}} + 3.30\,\mathrm{kW}, & p_{\mathrm{DCB}} < 0\,\mathrm{W} \end{cases} \\
p_{\mathrm{l,DCDC,1hb}} &= \begin{cases} 6.32\,\mathrm{m\Omega} \cdot {i_{\mathrm{SCES}}}^2 + 4.50\,\mathrm{V} \cdot i_{\mathrm{SCES}} + 0.45\,\mathrm{kW}, & i_{\mathrm{SCES}} \geq 0\,\mathrm{A} \\ 6.24\,\mathrm{m\Omega} \cdot {i_{\mathrm{SCES}}}^2 - 4.43\,\mathrm{V} \cdot i_{\mathrm{SCES}} + 0.45\,\mathrm{kW}, & i_{\mathrm{SCES}} < 0\,\mathrm{A} \end{cases} \\
p_{\mathrm{l,DCDC,2hb}} &= \begin{cases} 3.16\,\mathrm{m\Omega} \cdot {i_{\mathrm{SCES}}}^2 + 4.53\,\mathrm{V} \cdot i_{\mathrm{SCES}} + 0.79\,\mathrm{kW}, & i_{\mathrm{SCES}} \geq 0\,\mathrm{A} \\ 2.94\,\mathrm{m\Omega} \cdot {i_{\mathrm{SCES}}}^2 - 4.41\,\mathrm{V} \cdot i_{\mathrm{SCES}} + 0.79\,\mathrm{kW}, & i_{\mathrm{SCES}} < 0\,\mathrm{A} \end{cases} \\
p_{\mathrm{l,DCDC,3hb}} &= \begin{cases} 1.91\,\mathrm{m\Omega} \cdot {i_{\mathrm{SCES}}}^2 + 4.76\,\mathrm{V} \cdot i_{\mathrm{SCES}} + 1.02\,\mathrm{kW}, & i_{\mathrm{SCES}} \geq 0\,\mathrm{A} \\ 1.73\,\mathrm{m\Omega} \cdot {i_{\mathrm{SCES}}}^2 - 4.78\,\mathrm{V} \cdot i_{\mathrm{SCES}} + 1.03\,\mathrm{kW}, & i_{\mathrm{SCES}} < 0\,\mathrm{A} \end{cases}
\end{aligned}
$$

TABLE III: SCES model parameters.

L in µH	k_0 in µF/V	R_0 in mΩ	$C_{0,\mathrm{const}}$ in F	$R_{\mathrm{p},1}$ in Ω	$C_{\mathrm{p},1}$ in F	$R_{\mathrm{p},2}$ in Ω	$C_{\mathrm{p},2}$ in F	$R_{\mathrm{s},1}$ in mΩ	$C_{\mathrm{s},1}$ in F	R_{leak} in Ω
1.334	17.323	35.247	25.659	2.493	1.820	3.085	1.450	4.2717	11.673	675

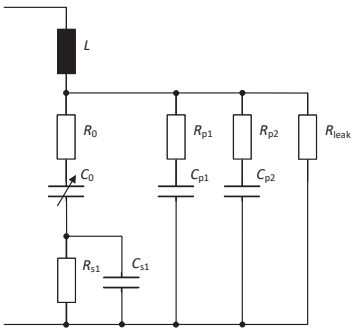

Fig. 3: Model for determining the electrical quantities of the SCES.

can also be derived from the current of the SCES. However, the initial voltage must be known for this.

IV. Measurements and Model Validation

1) Measurement Method: The measurement of the test bench was conducted with the data acquisition system *HBM GEN7tA* at a sample rate of $1\,\mathrm{MS/s}$. The measured currents and voltages are shown in Fig. 2. The current i_{SCES} was determined from the sum of the three choke currents of the DC/DC converter. For the measurements, the test bench was operated with an emulated ideal $400\,\mathrm{V}$ grid, which was provided by the Power Hardware In the Loop Lab [10] of the Energy Lab 2.0 [5].

The measurement of the whole system was performed with constant current constant power charge and discharge cycles (CC/CP-cycle). Thereby, the power at the terminals of the SCES is limited to $400\,\mathrm{kW}$ and the current limit of the SCES i_{SCES} for CC/CP-cycle n corresponds to $I_{\mathrm{SCES},n,limit} = n \cdot 100\,\mathrm{A}$. Each CC/CP-cycle consists of 5 phases:

1) charge from $100\,\mathrm{V}$ to $540\,\mathrm{V}$
2) $20\,\mathrm{s}$ pause
3) discharge from $540\,\mathrm{V}$ to $100\,\mathrm{V}$
4) $19\,\mathrm{s}$ pause
5) balance to $100\,\mathrm{V}$

After one cycle is finished, the next one is started directly. As an example for a single cycle, the current and voltage characteristics of the SCES for CC/CP-cycle no. 5 are shown in Fig. 4. The terminal voltage of the SCES is load-dependent. To approximate the open circuit voltage, we assume that the SCES is a voltage source with internal resistance. Thus, the internal voltage can be calculated with

$$u_{\mathrm{SCES,terminal}} = u_{\mathrm{SCES,internal}} + R \cdot i_{\mathrm{SCES}} \tag{6}$$

The resistance was determined by a step of the current from $0\,\mathrm{A}$ to $1400\,\mathrm{A}$ and calculated from the change in current and voltage, which results in $R = 39.99\,\mathrm{m\Omega}$. So the charging or discharging stops if the calculated no load voltage $u_{\mathrm{SCES,internal}}$ equals the desired value of $540\,\mathrm{V}$ resp. $100\,\mathrm{V}$. Using this method for determining the end of charging or discharging leads to an error between the desired and measured voltage of less than $3\,\mathrm{V}$ after charging or discharging has finished for more than $10\,\mathrm{s}$. The constant CC/CP-cycle were measured with 1 to 3 active half-bridges. Due to the maximum permitted phase current, 5 cycles for 1 active half-bridge, 10 cycles for 2 active half-bridges and 14 cycles for 3 active half-bridges where measured. For the complete measurement with 3 active half-bridges, i_{SCES} and u_{SCES} are depicted in Fig. 5. All the data in the following sections is based on the measurement data of the CC/CP-cycles.

2) Converter Power Losses: Fig. 6 shows the losses of the AFE including LCL filter and the DC/DC converter including

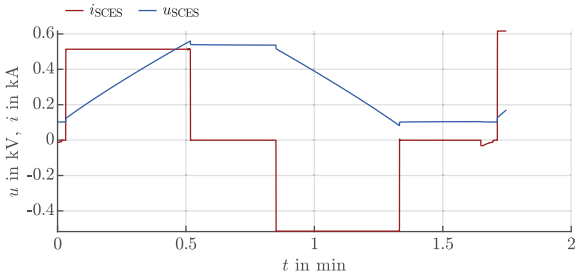

Fig. 4: CC/CP-cycle no. 5 with 3 active half-bridges.

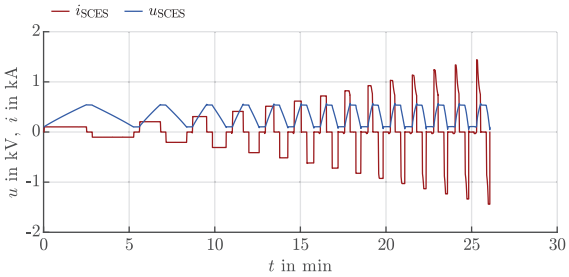

Fig. 5: CC/CP-cycle with 3 active half-bridges.

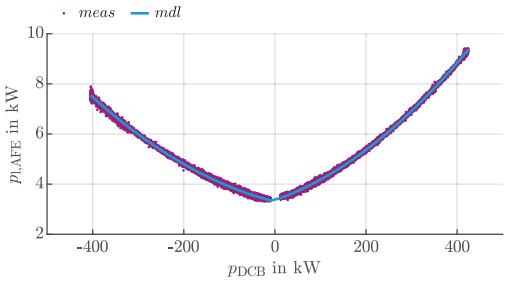

(a) Power loss of the AFE including the LCL filter as a function of the transmitted power.

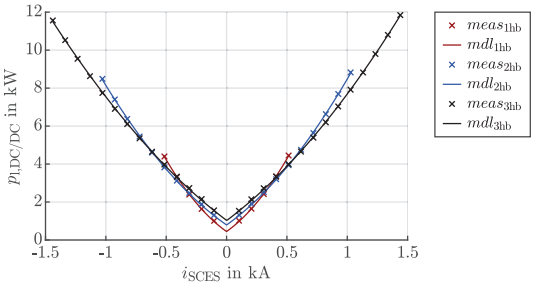

(b) Power loss of the DC/DC converter including its chokes as a function of the output current.

Fig. 6: Measured and modeled power losses of AFE andDC/DC converter.

inductors. The curves marked with meas represent values determined from measurements. Additionally, all lines marked with mdl are modeling results of the respective losses.

In Fig. 6a the losses of the AFE are shown. The data points with index mdl represent the AFE power dissipation averaged over a 20 ms window length for all 14 cycles with three active half-bridges during charging and discharging of the SCES. The associated characteristic curve with the index fit was determined with the averaged values using a least-squares estimator. The corresponding function is given in II. The asymmetry between positive and negative power losses is due to the voltage drop of the LCL filter, which results in higher AC currents at the AFE for charging than for discharging the SCES. Fig. 6b shows the losses of the DC/DC converter with one (1hb), two (2hb) or three (3hb) active half-bridges. The power dissipation characteristic of the DC/DC converter was determined by averaging the power dissipation over each charge or discharge process. However, only the constant current range was averaged. The resulting average values were then used to determine the characteristic curve with a least-squares estimator. The losses can be reduced considerably at some operating points by switching off individual half-bridges, but this is not advantageous at all possible operating points. The lowest losses occur in the range of $-350\,\mathrm{A}$ to $350\,\mathrm{A}$ for one active half-bridge, for $-600\,\mathrm{A}$ to $-350\,\mathrm{A}$ and $350\,\mathrm{A}$ to $500\,\mathrm{A}$ for two active half-bridges and for currents smaller than $-600\,\mathrm{A}$ and larger than $500\,\mathrm{A}$ for three active half-bridges.

3) Loss Energy: In the following, the loss energy of the measurements and the associated modeling error of AFE, DC/DC converter and SCES for the CC/CP-cycles is considered. To determine the energy of a CC/CP-cycle, the power is integrated over the complete cycle. These are shown in Fig. 7. The model error is always calculated as the measured value minus the modeled value. The seemingly reduced losses of the last cycle of each measurement series arise from the termination of the measurement cycle before restoring the voltage to $100\,\mathrm{V}$. This can be reasonably represented for the inverter losses with the measurement and modeling. However, for the SCES loss energy, this results in an error because the voltage between the beginning and end of the cycle differs. For all cycles, the model errors of the loss energy of AFE and DC/DC converter, respectively, are each smaller than $3\,\mathrm{W\,h}$ (Fig. 7a-7d). Fig. 7e shows the loss energy of the SCES. Since the number of active half-bridges has only a very small influence on the loss energy in the SCES, only the measurement results for three active half-bridges are depicted. In addition, the losses of the model with 1 to 3 active half-bridges are shown. Furthermore, $mdlR, 3p$ displays the loss energy assuming the losses of the SCES would be determined with the resistance R in Eq. 6, which was used to determine the internal voltage of the SCES. This approach shows a significant deviation from the measured loss energy of the SCES and is thus unsuitable for modeling. In Fig. 7f the model errors for 1 to 3 active half-bridges are shown. The first cycle with an active half-bridge has the largest model error. This is due to the fact that the voltage of the SCES was previously at about $100\,\mathrm{V}$ for a very long time and that the model does not represent very low-frequency components of the real behavior of the SCES. In addition, the model was fed the average values of the currents per pulse period, which means that the additional losses due to the ripple of the current cannot be represented. This leads to an increase of the error especially for the measurements with one active half-bridge. Except for the first cycle with an active half-bridge and the last cycles of all measurement series, the maximum model error is below $8\,\mathrm{W\,h}$, which corresponds to less than $0.6\,\%$ of the retrievable energy of the SCES and agrees well with the measurement.

4) SCESS Energy: Fig. 8 shows the energies of the total system at the grid for the CC/CP-cycles. The index charge describes the energy supplied from the grid during the charging

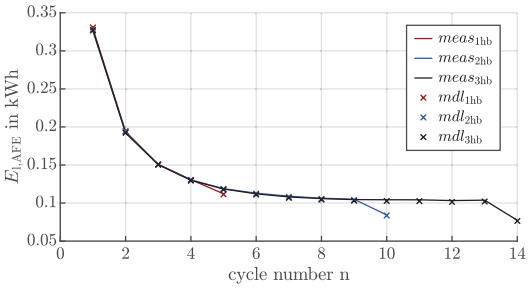

(a) Loss energy of the AFE including the LCL filter.

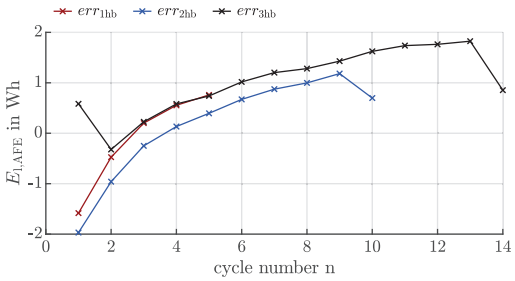

(b) Loss energy error of the AFE including the LCL filter.

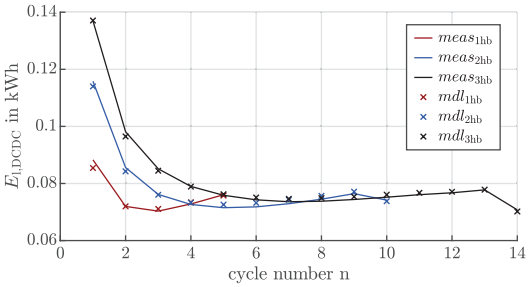

(c) Loss energy of the DC/DC converter.

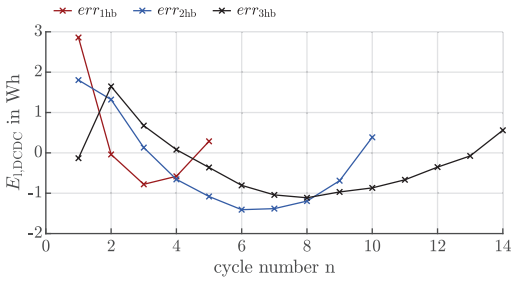

(d) Loss energy model error of the DC/DC converter.

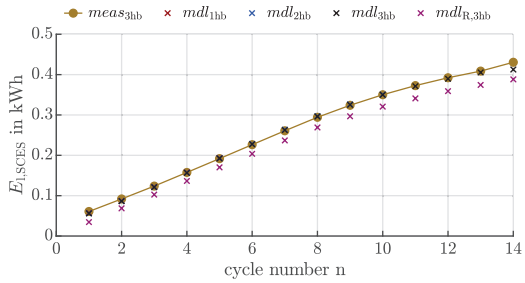

(e) Loss energy of the SCES.

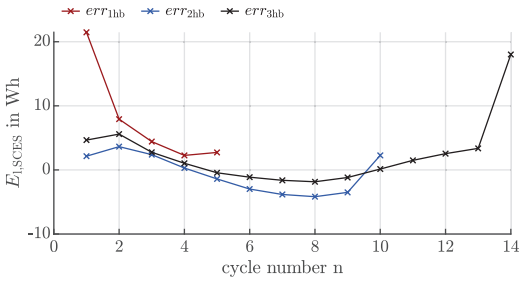

(f) Loss energy model error of the SCES.

Fig. 7: Energy losses of measurement and model (left side) and model error (right side) of the AFE, DC/DC converter and SCES for the CC/CP-cycles.

process. The index discharge describes the energy fed back into the grid during discharging and loss corresponds to the losses during the full CC/CP-cycle. The graph shows both the measured and the modeled values with 3 active half-bridges. For all measuring points a very high match between the modeled and the measured values is given.

5) Limits of modeling: The modeling does not correctly represent the current ripple losses in the DC/DC converter, since these losses depend on the modulation factor and the modeling only considers the current amplitude. Modeling only considers the current amplitude. The current ripple also leads to losses in SCES that are not taken into account. Due to the limited integration time for the determination of the energy, there are inaccuracies for the very low frequency behavior of the SCES which can be seen by the energy error for cycle number 1 with one active half-bridge in Fig. 7f. Compared to the system losses, this inaccuracy is very small. Different grid conditions with unbalances, harmonics or a change in the grid voltage cannot be represented either.

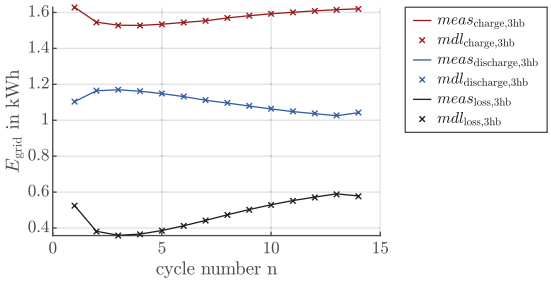

Fig. 8: Measured and determine charge and discharge energy and energy loss of the complete test bench for the CC/CP-cycle, with 3 active half-bridges.

V. Modeling of Constant Power Charging and Discharging Cycles

After showing in the previous chapters that the chosen model approach of the SCES is suitable to model the power and energy at the grid connection point, the modeling approach is used to investigate the behavior of the SCES for constant power cycles (CP-cycle) with constant grid power p_{grid}. The considerations in this section are based on modeling with 3 active half-bridges. During the CP-cycles, the SCES is charged from the initial voltage $u_{\mathrm{SECS,min}}$ to 540 V and then discharged back to $u_{\mathrm{SECS,min}}$. This was simulated with $u_{\mathrm{SECS,min}}$ from 100 V to 450 V in 50 V increments and for the grid power p_{grid} from 25 kW to 325 kW in 25 kW increments. In Fig. 9 the required energy to charge the SCES from the starting voltage $u_{\mathrm{SECS,min}}$ to 540 V is shown ($E_{\mathrm{grid,charge}}$). In addition, the loss energy $E_{\mathrm{l,grid}}$ for a complete cycle is shown in red.
In Fig. 10 the energy returned to the grid during discharge is shown ($E_{\mathrm{grid,discharge}}$). In addition, the time $t_{\mathrm{discharge}}$ in which the desired power can be delivered to the grid is displayed in red. In Fig. 9 and Fig. 10 no values are given if the desired power cannot be reached over the complete cycle.

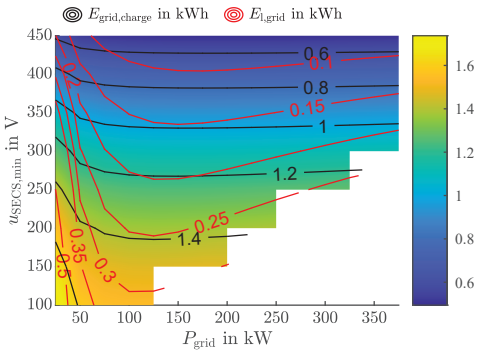

Fig. 9: Charge energy and full cycle loss energy for the modeled CP-cycles.

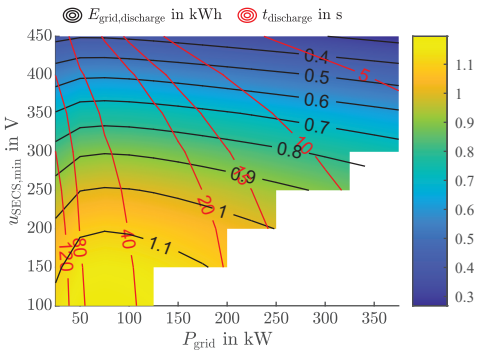

Fig. 10: Discharge energy and time for the modeled CP-cycles.

VI. Conclusion

In this paper, a supercapacitor based test bench was presented. The losses of the AFE, the DC/DC converter and the SCES were measured. It was shown that switching off half-bridges of the DC/DC converter in parts of the operating range can significantly reduce its losses. Mathematical descriptions of the operating point-dependent power losses as well as a model of the SCESS were presented and compared with the measurement results. From this, a model was developed which determines the power flows and losses in the overall system as a function of the current and the voltage of the SCES. The results show that the model is suitable for representing the losses of the components and the overall system. Constant power cycles were simulated and allow to evaluate the suitability of the storage system for different load profiles. In a next step, the model could be used to optimize the operation of the SCESS. Also, the model can be extended to take into account the losses of the current ripple.

References

[1] N. Orth, N. Munzke, J. Weniger, C. Messner, R. Schreier, M. Mast, L. Meissner, and V. Quaschning, "Efficiency characterization of 26 residential photovoltaic battery storage systems," *Journal of Energy Storage*, vol. 65, p. 107299, 2023.

[2] X. Luo, J. Wang, M. Dooner, and J. Clarke, "Overview of current development in electrical energy storage technologies and the application potential in power system operation," *Applied Energy*, vol. 137, pp. 511–536, 2015.

[3] S. Guo, Y. Yao, L. Hu, B. Sun, H. Chai, R. Huang, and J. Zhao, "Energy storage technology and its typical application in new energy grid connection system," in *2020 IEEE Sustainable Power and Energy Conference (iSPEC)*. IEEE, 2020, pp. 1969–1974.

[4] B. Schmitz-Rode, L. Stefanski, R. Schwendemann, S. Decker, S. Mersche, P. Kiehnle, P. Himmelmann, A. Liske, and M. Hiller, "A modular signal processing platform for grid and motor control, hil and phil applications," in *2022 International Power Electronics Conference (IPEC-Himeji 2022- ECCE Asia)*. IEEE, 2022, pp. 1817–1824.

[5] V. Hagenmeyer, H. Kemal Çakmak, C. Düpmeier, T. Faulwasser, J. Isele, H. B. Keller, P. Kohlhepp, U. Kühnapfel, U. Stucky, S. Waczowicz, and R. Mikut, "Information and communication technology in energy lab 2.0: Smart energies system simulation and control center with an open-street-map-based power flow simulation example," *Energy Technology*, vol. 4, no. 1, pp. 145–162, 2016.

[6] A. Wintrich, U. Nicolai, W. Tursky, and T. Reimann, *Application manual power semiconductors*. Ilmenau: ISLE-Verl., 2011.

[7] G. Asher, C. Klumpner, M. Rashed, and P. Kulsangcharoen, "A new duty cycle based efficiency estimation method for a supercapacitor stack under constant power operation," in *5th IET International Conference on Power Electronics, Machines and Drives (PEMD 2010)*. Institution of Engineering and Technology, 2010, p. 243.

[8] P. Kulsangcharoen, C. Klumpner, M. Rashed, G. Asher, G. Z. Chen, and S. A. Norman, "Assessing the accuracy of loss estimation methods for supercapacitor energy storage devices operating under constant power cycling," in *Power Electronics and Applications EPE'14-ECCE 26-28 August 2014*, 2014, pp. 1–11.

[9] M. Hetzel, "Supercapacitor modeling and parameter identification of a 400 kw grid-connected supercapacitor energy storage system using the inherent impedance spectroscopy capability of its dc/dc converter: preprint," *IEEE Energy Conversion Congress and Exposition, ECCE 2023 (preprint)*, 2023.

[10] G. de Carne and D. Kottonau, "Power hardware in the loop laboratory testing capability for energy technologies," in *2022 AEIT International Annual Conference 03-05 October 2022*, 2022, pp. 1–5.